Microfluid Nanofluid (2015) 18:9–18
DOI 10.1007/s10404-014-1420-0

RESEARCH PAPER

Multicomponent phase transition kinetics in cereal foam—part II: impact of microstructural properties

S. Mack · M. A. Hussein · T. Becker

Received: 25 November 2013 / Accepted: 25 April 2014 / Published online: 15 May 2014

Abstract In the bakery industry, a considerably high amount of energy is used for the baking process. A possibility to decrease the baking time by means of optimized heat transfer through the bread microstructure would lead to less required baking time and cost reduction. Thermal treatment of cereal foam implicates thermo-physical processes such as simultaneous heat and mass transfer associated with evaporation–condensation-based heat transfer through the bubbles. Numerical investigations are carried out to deliver sophisticated insight into the heat transfer processes at microscale, supporting process understanding and visualization of phenomena inside the foam bubbles. In a further step, the elaborated knowledge is employed to determine the main influencing parameter on the heat transfer through the foam microstructure by means of lattice Boltzmann modeling techniques. For optimization purposes, the microstructure as well as individual foam lamella configurations are considered in the parameter variation studies.

Keywords Numerical modeling · Lattice Boltzmann · Phase transitions · Cereal foam · Thermo-physics · Heat and mass transfer

1 Introduction

In cereal foam microstructures, heat transfer is suggested to depend to a high degree on evaporation–condensation processes inside the foam bubbles (Sablani et al. 1998; Thorvaldsson and Janestad 1999; Purlis and Salvadori 2009). This cyclic process is depending on heat and vapor transfer, as well as the associated transfer of latent heat. Heat is transferred through the foam lamella; considering an individual foam bubble surrounded by the lamella, water evaporates at the warmer side of the bubble, thereby absorbs latent heat of vaporization, diffuses through the bubble, and condenses again depending on the local conditions with release of the latent heat (de Vries et al. 1989; Wagner et al. 2007). This hypothesis is based on experimental investigations as well as on basic physical principles, where conclusions can be drawn based on the following considerations:

(i) Heat transfer proceeds quicker in fermented than in unfermented dough during the baking process (de Vries et al. 1989).
(ii) Cereal foam structure can be considered analogous to a heat pipe, where present water evaporation and condensation overtakes the major role of heat transfer (Sluimer and Krist-Spit 1987)
(iii) Temperature inside bread during baking reaches a plateau of 100 °C (Thorvaldsson and Skjöldebrand 1998)
(iv) Moisture transport toward the coldest spot of the loaf can be recorded (Thorvaldsson and Janestad 1999; Wagner et al. 2007)

Several researches are carried out to measure temperature and humidity distributions during baking (Zanoni and Peri 1993; Thorvaldsson and Janestad 1999; Wählby and Skjöldebrand 2001; Wagner et al. 2007; Purlis and Salvadori 2009). Temperature distributions during baking are well known, but vapor diffusion in combination with phase transitions kinetics is currently poorly reported. In particular, the high-temperature conditions impede the

S. Mack (✉) · M. A. Hussein · T. Becker
Group of (Bio-) Process Analysis, Faculty of Life Science Engineering, Technische Universität München, Weihenstephaner Steig 20, 85354 Freising, Germany
e-mail: s.mack@wzw.tum.de

measurement conditions. In addition, the complex microstructural characteristics of cereal foam and the occurrence of the phenomena of interest in the microscale yield to unfeasible measurement conditions. Therefore, it is not surprising that mismatching findings are the current state of research. On the one hand, moisture transfer toward the coldest spot is reported (Thorvaldsson and Janestad 1999; Wagner et al. 2007), and on the other hand, no moisture change inside the crumb was found (Zanoni and Peri 1993). Besides such drawbacks, the main challenge still remains: the small length scale and to get insight into processes inside the bubbles.

Promising options are numerical modeling techniques, offering the possibility to deliver insight without destroying or influencing the process. In recent researches, focus was set to simultaneous heat and mass transfer based on macroscopic descriptions of the processes. Thus, microstructural and material properties, as well as physical phenomena such as evaporation–condensation, are regarded as continuum quantities (Zanoni and Peri 1993; Purlis and Salvadori 2009). To gain insight into the processes at the mesoscale, the lattice Boltzmann method (LBM) proved to be a powerful tool, bridging micro- and macroscales (Zhang 2011). A simplified foam structure was used to model simultaneous heat and mass transfer through cereal foam under thermal treatment by the use of LBM, where heat transfer and mass transfer were regarded to depend only on heat and mass diffusion (Hussein and Becker 2010). The influence of material properties was subject of a further study, where thermal diffusivity of the foam lamella was varied in a realistic foam geometry based on μCT-images, showing that higher thermal diffusivity increases the heat transfer rate (Mack et al. 2013a). These previous researches miss the implementation of evaporation–condensation processes, but build the basis for the current study. The objective of this work is the application of a recently developed lattice Boltzmann algorithm, considering the specific saturation conditions of water vapor, including phase transitions of water vapor to condensed vapor beyond saturation and vice versa. Furthermore, the associated uptake and release of latent heat depending on the amount of transitioned species are considered. Following the length scale of the foam, as given in Fig. 1, the simulations are carried out in the order of mm length scale. In a further step, the algorithm is used for an intensive parameter variation study elaborating the impact of microstructural properties on the heat transfer. The parametric investigations cover (1) porosity variations of the crumb, (2) variations of foam lamella, and (3) cross-correlations of varied thermal diffusivity of the foam lamella in dependence of the varied microstructural characteristics. These parametric investigations allow an estimation of the main influencing parameter on enhanced heat transfer. The results can then be used to support experimental research to transfer the virtual elaborated main influencing parameter to the real baking process.

2 Materials and methods

2.1 Lattice Boltzmann diffusion modeling in combination with phase transitions

The applied lattice Boltzmann equation is given in Eq. 1 (Succi 2001; Sukop and Thorne 2007), where f represents the particle distribution function, $\boldsymbol{x}$ is the space in x direction, e is the unit vector, t is the time, δt is the time step, $\boldsymbol{e}$ is the unit vector, Ω_i is the collision operator, and F_i an external sink or source term.

$$f_i(\mathbf{x} + \mathbf{e}\delta t, t + \delta t) = f_i(\mathbf{x}, t) + \Omega_i(\mathbf{x}, t) + F_i \tag{1}$$

The proposed lattice Boltzmann algorithm is based on coupled heat and vapor diffusion. Therefore, two separate equations for each property are solved simultaneously, the temperature distribution T and the vapor distribution V, respectively, see Eq. 2.

$$f_i = \begin{bmatrix} T_i \\ V_i \end{bmatrix}; \ \Omega_i = \begin{bmatrix} -\frac{1}{\tau_T}(T_i - T_i^{\mathrm{eq}}) \\ -\frac{1}{\tau_V}(V_i - V_i^{\mathrm{eq}}) \end{bmatrix} \tag{2}$$

The collision operator Ω accounts for particle to particle interactions, where the particle distribution function relaxes toward a local equilibrium f^{eq}, according to the specific relaxation time τ (Succi 2001) as given in Eq. 3.

$$\Omega_i(f(\mathbf{x}, t)) = -\frac{f_i(\mathbf{x}, t) - f_i^{\mathrm{eq}}(\mathbf{x}, t)}{\tau} \tag{3}$$

The equilibrium distribution function is shown in Eq. 4 for diffusion, where under the assumption of zero velocity flow, the original Maxwellian velocity distribution diminishes (Hussein and Becker 2010).

$$f_i^{\mathrm{eq}} = w_i f \tag{4}$$

The relaxation time for each process is related to the thermal diffusivity according to Eq. 5 (Wolf-Gladrow 2005).

$$\tau_T = 3\alpha + \frac{1}{2}; \ \tau_V = 3D + \frac{1}{2} \tag{5}$$

where α represents the thermal diffusivity and D is the vapor diffusivity. Evaporation boundaries are implemented at the lamella–bubble interface and as well at the vapor-condensed vapor boundary. The evaporation rate is calculated based upon the partial vapor pressure dependent according to Langmuirs' equation, given in Eq. 6.

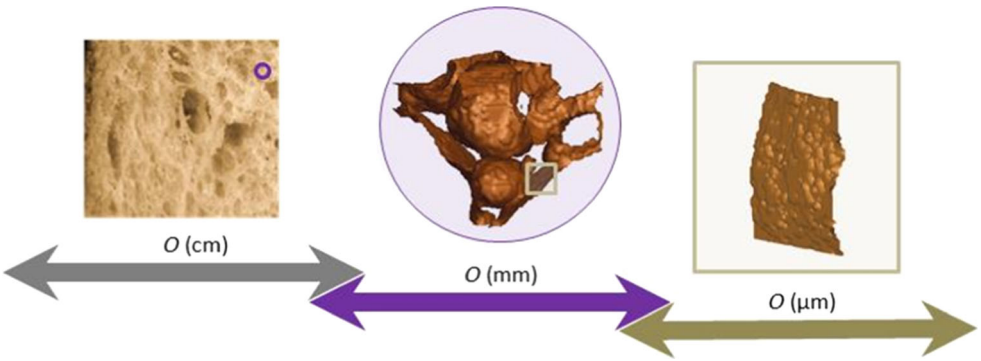

Fig. 1 Length scale of cereal foam, showing from *left* to *right* macro-, meso- and microstates of the foam with corresponding orders of length scales (O), thus showing the length scale of product (O cm), its composition of bubbles and lamella (O mm), as well as a single lamella (O µm)

$$\frac{\mathrm{d}V}{\mathrm{d}t} = (P_\infty - P_{\mathrm{Gas}})\sqrt{\frac{m}{2\pi k T}} \tag{6}$$

$\mathrm{d}V/\mathrm{d}t$ is the flux of vaporized water, P_∞ is the vapor pressure of lamella water and condensed vapor, respectively, P_{Gas} is the partial vapor pressure of the vapor in the gas, m is the mass of water, k is the Boltzmann constant, and T the temperature in °C. In addition, the current temperature, vapor density as well as saturation conditions are calculated locally, which constitute the framework of phase transition processes and the development of an additional mass source term C representing the condensed vapor, Eq. 7.

$$f_i = \begin{bmatrix} T_i \\ V_i \\ C_i \end{bmatrix} \quad \begin{cases} -H_i & (\mathrm{d}v > 0) \\ +H_i & (\mathrm{d}C > 0) \\ -S_i & (V > V_{\mathrm{Sat}}) \\ +S_i & (V > V_{\mathrm{Sat}}) \end{cases} \tag{7}$$

The external sink and source term F extends the equation to take phase transition into account. F is composed of two individual parts, S is the source of transitioned species, whereas H represents the amount of absorbed or released heat, see Eq. 8.

$$F_i = \begin{bmatrix} H_i \\ S_i \end{bmatrix} \tag{8}$$

Macroscopic values are recovered according to the relation given in Eq. 9, where ρ is the macrodensity (Sukop and Thorne 2007).

$$\rho = \sum_i f_i \tag{9}$$

Linkage between the processes in SI units and the lattice domain is given by similarity considerations. Meaning that, the Fourier and the Lewis number are applied as non-dimensional parameters to ensure similarity conditions. Hence, SI units can be transferred according to Eq. 10 to lattice units (LU) and vice versa.

$$\text{Conversion factor} = \frac{\text{Value}_{\mathrm{SI}}}{\text{Value}_{\mathrm{LU}}} \tag{10}$$

2.2 Computational domain

The computational domain is generated based upon a stack of µCT-images of bread to enable realistic insight into cereal foam microstructures. A detailed description of dough manufacture and µCT-imaging is provided by Dietrich et al. (2012). The µCT-images are uploaded in the Boltzmann code where an edge detection algorithm (Perez Alvarado et al. 2011) is applied to distinguish between foam lamella and foam bubble. Figure 2 shows the computational domain of a three-dimensional 2 × 2 × 2 mm foam domain. Inner-bubble surfaces are displayed with the grid. Foam bubble diameter is in the range of 1 mm, whereas the cross-sectional thickness of foam lamella is ∼200 µm.

2.3 Modeling assumptions and initial conditions

The modeling domain is composed of two foam components, the lamella and the bubbles. The foam lamella consists of a water–starch–gluten network, where the specific material properties are calculated and applied in the simulations based on bread dough properties:

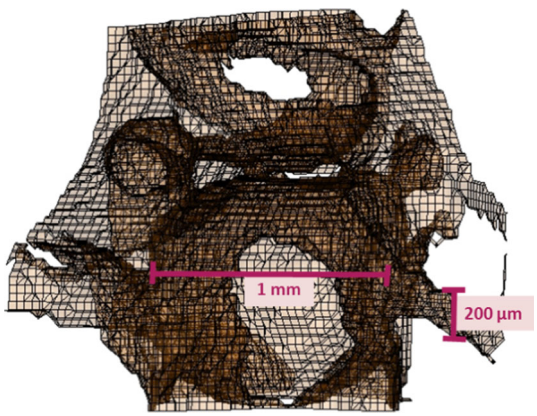

Fig. 2 Computational domain of the cereal foam, showing the mesh domain of a bubble which size is of approximately 1 mm, and foam lamella thickness of ∼200 µm

(i) The thermal ($\alpha = 0.157 \times 10^{-6}$ m^2/s) and the mass diffusivity ($D = 3.0 \times 10^{-9}$ m^2/s), at a temperature of 100 °C, of the lamella are based on properties for unfermented dough.
(ii) The thermal ($\alpha = 0.0192 \times 10^{-3}$ m^2/s) and mass diffusivity ($D = 0.02 \times 10^{-3}$ m^2/s), at a temperature of 100 °C, for the bubble component are based on water vapor properties.

The bubbles are regarded to be filled exclusively with water vapor, where additional gases are neglected due to their minor content. Initial relative humidity at 30 °C is 92.2 %. The initial values are taken from previously published experimental data (Mack et al. 2013b). The proposed LB algorithm so far considers the phase transition depending on the temperature-dependent saturation conditions of water vapor. This implies that the amount of vapor which is locally present and exceeds the temperature-dependent saturation limit undergoes a phase change and the condensed vapor phase develops, resulting in a wet steam region, composed of liquid droplets, rather than a continuous liquid phase. Depending on the amount of transitioned vapor, the corresponding amount of heat is added to the heat equation. Thus, the processes being of impact on the heat transfer are regarded in the current model.

2.4 Parameter variations

The upload of the μCT-images and their linkage to the modeling domain is depending on a specific threshold used in the edge detection algorithm, to distinguish between gas phase and lamella. Lowering or increasing this threshold virtually offers the possibility to change the virtual crumb structure by means of pore size, lamella thickness, and increasing amount of voids in the lamella, whereas the general crumb structure remains similar. Due to this procedure, the microstructural changes are related to porosity variations, which are shown in Table 1.

The slightly differing microstructures are used to carry out parameter variation studies. Figure 3 shows the computational domain of each variation case. The inner iso-surfaces of cereal foam bubbles are illustrated in brown. A heat source is implemented on the right-hand side, shown by the red plane, see Fig. 3a, b. To emphasize the microstructural changes, Fig. 3b shows slices through the middle of the modeling domain. Drawback of this method is that bubble size, lamella size, and the occurrence of microvoids are always directly linked to a different porosity, thus allowing conclusions on the heat transfer depending on porosity. If amount of lamella, bubble size, lamella thickness, or microvoids themselves are influencing the heat transfer rate and to which amount is not possible.

Table 1 Crumb structure variations depending on the threshold

Threshold	Porosity (%)
8	66.7
9	69.4
10	72.1
11	74.8
12	77.5

To overcome such drawbacks, a further parameter variation study is carried out focusing on the constitution of the lamella. The variation study considers an individual lamella, without and with increasing amount of similar sized voids and as well increasing size of a single void. The lamellas are generated artificial allowing a constant amount of mass, even though the constitution is varied. Furthermore, the amount of voids from 0 to 6 satisfies a similar increase of void space from 0 to 6 LU as the void size from 0 to 6. The parameter variation cases are focusing on microstructural properties, whereas additionally the thermal diffusivity of the foam lamella is varied in a realistic range for cereal dough, as summarized in Table 2. The combined implementation of material as well as microstructural properties offers the possibility to estimate which property overtakes the leading role by means of heating times reduction.

3 Results and discussion

3.1 Simulation results

Contour plots of temperature and vapor distribution are shown in Fig. 4a and b for proceeding time steps at a porosity of 72 %. In addition, the development of condensing vapor as well as its re-evaporation is shown in Fig. 4c. The computational domain consists of initially two components, the foam lamella and the foam bubbles. On the right-hand side, a heat source is implemented in the domain, resembling the heat flux from neighbor crumb sections with constant temperature of 100 °C. Figure 4a shows the temperature distribution through the domain, it can be seen, that heat flux through the bubbles proceeds quicker than through the foam lamella. This is reasoned by the higher thermal diffusivity of the vapor phase compared to the foam lamella, but as well due to the additional energy transfer based on the evaporation–condensation mechanism. The half-moon shaped temperature increase after 250 time steps inside the foam bubble is resulting from condensation next to the foam lamella–bubble interface. Due to concentration and partial vapor pressure gradients, water evaporates from the lamella, exceeding the saturation limit of the current temperature resulting in a phase

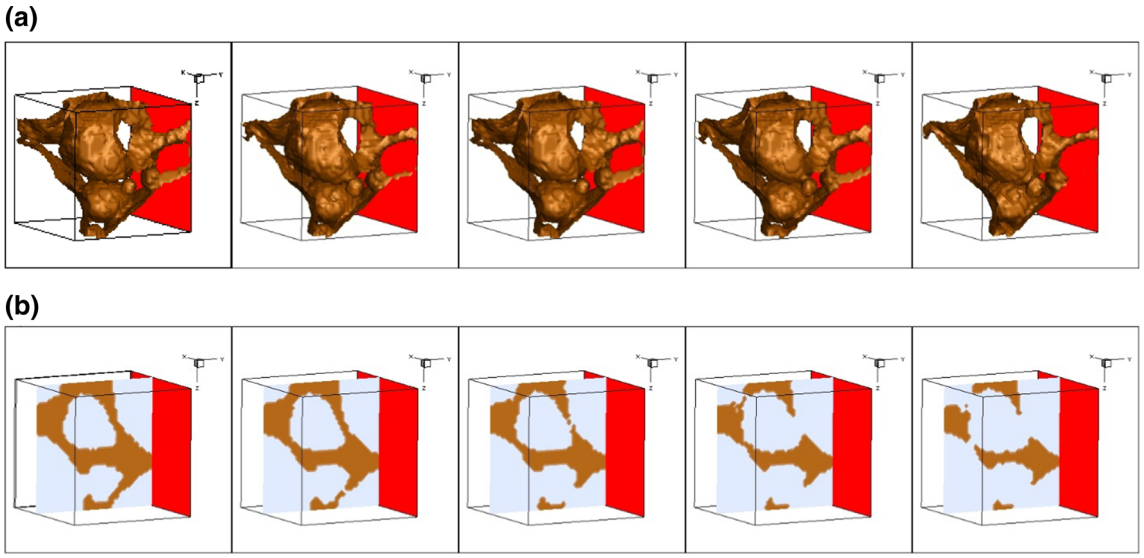

Fig. 3 Cereal foam microstructure variations, porosity increases from *left* to *right* from 66.7 to 77.5 %. **a** Three-dimensional illustration of a microstructure section, iso-surfaces of the foam bubbles are shown in *brown*, the heat source given in *red*. **b** Two-dimensional illustration in the middle of the microstructural section, emphasizing the differing lamella constitutions with increasing porosity

Table 2 Parameters variation cases of foam lamella sections

Parameter variations	Lattice units	SI units
Amount of voids	0–6	0–240 μm
Void size	0–6 LU	0–240 μm
Thermal diffusivity	1.1×10^{-3} m^2/s − 2.3×10^{-3} m^2/s	0.117×10^{-6} m^2/s − 0.197×10^{-6} m^2/s

Variation parameters are amount of voids, void size, and thermal diffusivity of the lamella

change and the thereby released energy of the previous vapor phase. At advanced time steps, both heat transfer mechanisms are hard to distinguish, reasoned by the simultaneous occurrence of thermal diffusion and evaporation–condensation-based heat transfer. After 20,250 time steps, the temperature reached a level of 98 °C, which is the end point of the simulation due to the fact that cereal foam structure solidifies at this temperature level and the baking process ends (Rask 1989; Zanoni and Peri 1993). The related time in SI units to reach end of baking can be derived from the value conversion as given in Eq. 10. The computational domain represents a $2 \times 2 \times 2$ mm-sized section of cereal foam; thus, the required time to heat the domain in SI units is 38 s. Extrapolating this to a customary product height of 10 cm would yield to a required baking time of 32 min. Since the simulations are straightly carried out in the crumb domain without considering crust and oven conditions which indeed influence baking time, this time only gives an estimation of the real heating time. Thus, the required heating time is given in time steps in the following.

The simultaneously solved vapor diffusion through the foam is shown in Fig. 4b. Vapor is diffusing through the bubbles as well as through the lamella, depending on the specific mass diffusion coefficients. At initial stages of the simulation, the amount of vapor is equally distributed among the foam bubbles, due to the initial conditions of a relative humidity of 92.2 % at a temperature of 30 °C. At time step 250, there is an increase of vapor visible at the right corner next to the foam lamella. This local increase of vapor in the gas phase is reasoned by the increasing temperature and thereby induced evaporation from the lamella toward the bubble. This effect can be tracked over the following time steps, resulting in an increase of vapor in the bubble phase. Thus, the vapor is evaporating depending on local temperature and therewith vapor pressure differences and diffusing through the bubbles.

The consequence of this temperature- and pressure-dependent vapor flux is shown in Fig. 4c. Depending on local amount of vapor, temperature and thus the local temperature-dependent saturation level, condensation occurs. The condensed vapor is illustrated in dark blue, and it can be seen that with proceeding time steps, the amount of condensed vapor increases according to the increasing amount of vapor in the bubbles. In addition, at the time steps 15,250 and 20,250, the re-evaporation can be seen by the decrease of condensed vapor. This re-evaporation occurs concisely at the final time steps due to the longer exposure of high temperature at this location associated with vapor displacement toward neighbor

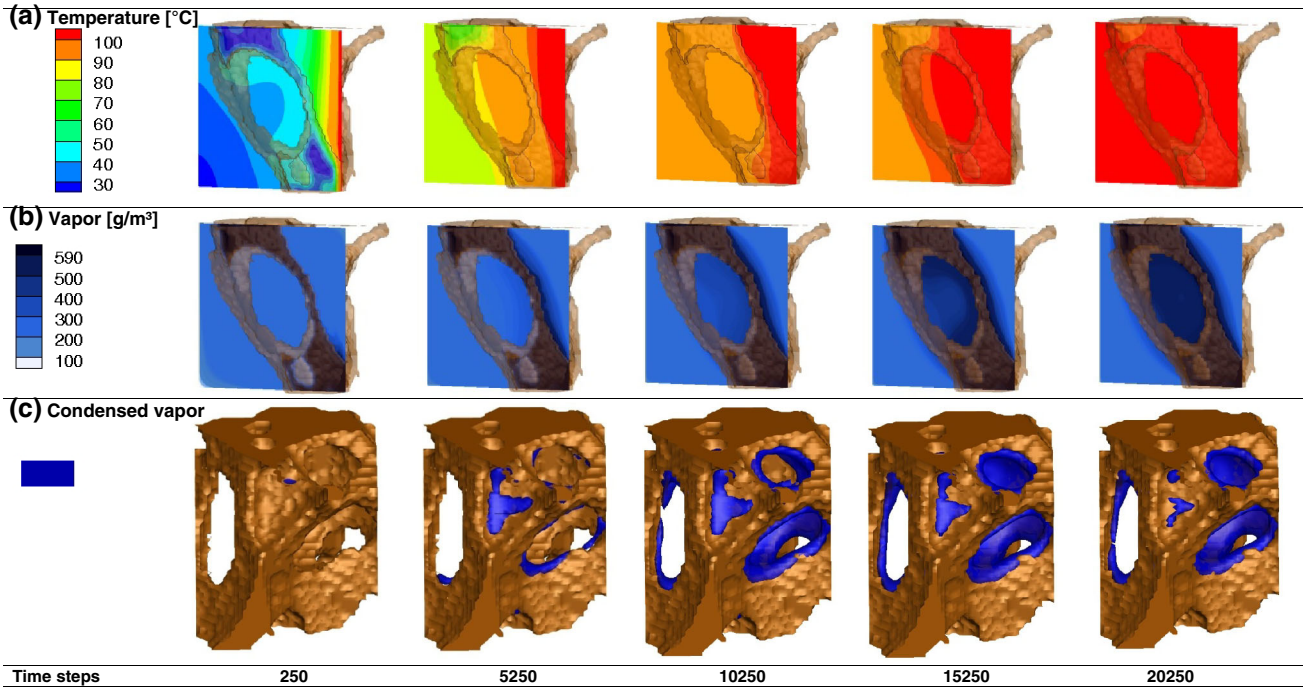

Fig. 4 Temperature, vapor, and condensed vapor distribution at proceeding simulation time steps in a foamed dough model structure

sections. Figure 5 shows the simulation results combined for heat flux, vapor diffusion, and evaporation–condensation. The temperature distribution is plotted at the crumb structure surface. The increasing evaporation front from the lamella toward the bubble phase is illustrated by a light gray-blue iso-surface, and the condensed vapor phase is shown by the dark blue layer.

The plots show the temperature flux through the domain, yielding to increased temperature-dependent evaporation from the lamella. An evaporation front is developing at the high-temperature regions at the right-hand side. Subsequently, an evaporation front is developing on the left-hand side as temperature increases. Reasoned by the increased amount of vapor in the bubbles, the amount of vapor which is locally beyond saturation condenses. According to local temperature and vapor pressure conditions, the previously condensed vapor re-evaporates again, visible at time step 20,250 on the right-hand side.

The evaporation–condensation mechanism includes evaporation from the lamella boundary, condensation inside the bubbles at the lamella–bubble interface, and re-evaporation from the condensed vapor. This cyclic evaporation–condensation occurs locally during the whole heating process as shown in Fig. 6. The plot shows the temperature (solid black line) dependent development of condensed vapor (solid pink line). Figure 6a–c shows the local amount of condensed vapor at the time steps 8,000, 8,500, and 9,000 at the lamella–bubble interface. At time step 8,000, the local amount of condensed vapor reached a local minimum due to re-evaporation of the condensed vapor. The proceeding evaporation from the lamella due to increasing temperature and therewith increasing vapor pressure gradients yields to local increase of vapor in the bubble and thus if the amount is beyond saturation, the vapor condenses, see Fig. 6b. At time step 9,000, again a local minimum is reached due to re-evaporation of the condensed vapor. This cyclic evaporation–condensation process continues until the local conditions change due to less available water present in the lamella as it can be seen in the final stages of the heating process after 20,000 time steps where the condensed vapor curve flattens.

3.2 The role of evaporation–condensation heat transfer

The simulation results show that besides thermal conduction, heat is transferred according to the evaporation–condensation mechanism. Reconsidering that evaporation–condensation yields to release of additional heat during condensation, but as well absorbs energy during vaporization yielding to isothermal phase change at macroscale, which is the basic feature of latent heat transfer. In theory, if heat transfer by evaporation–condensation is of minor impact and heat transfer is mainly depending on thermal diffusivity through each phase, then variations of the influencing parameters, such as thermal conductivity, specific heat, and density of the foam lamella, are the point of interest to reach higher heat transfer. On the opposite, if a high amount of heat is transferred by the evaporation–condensation mechanism, then different or additional parameter variations should be taken into account. If

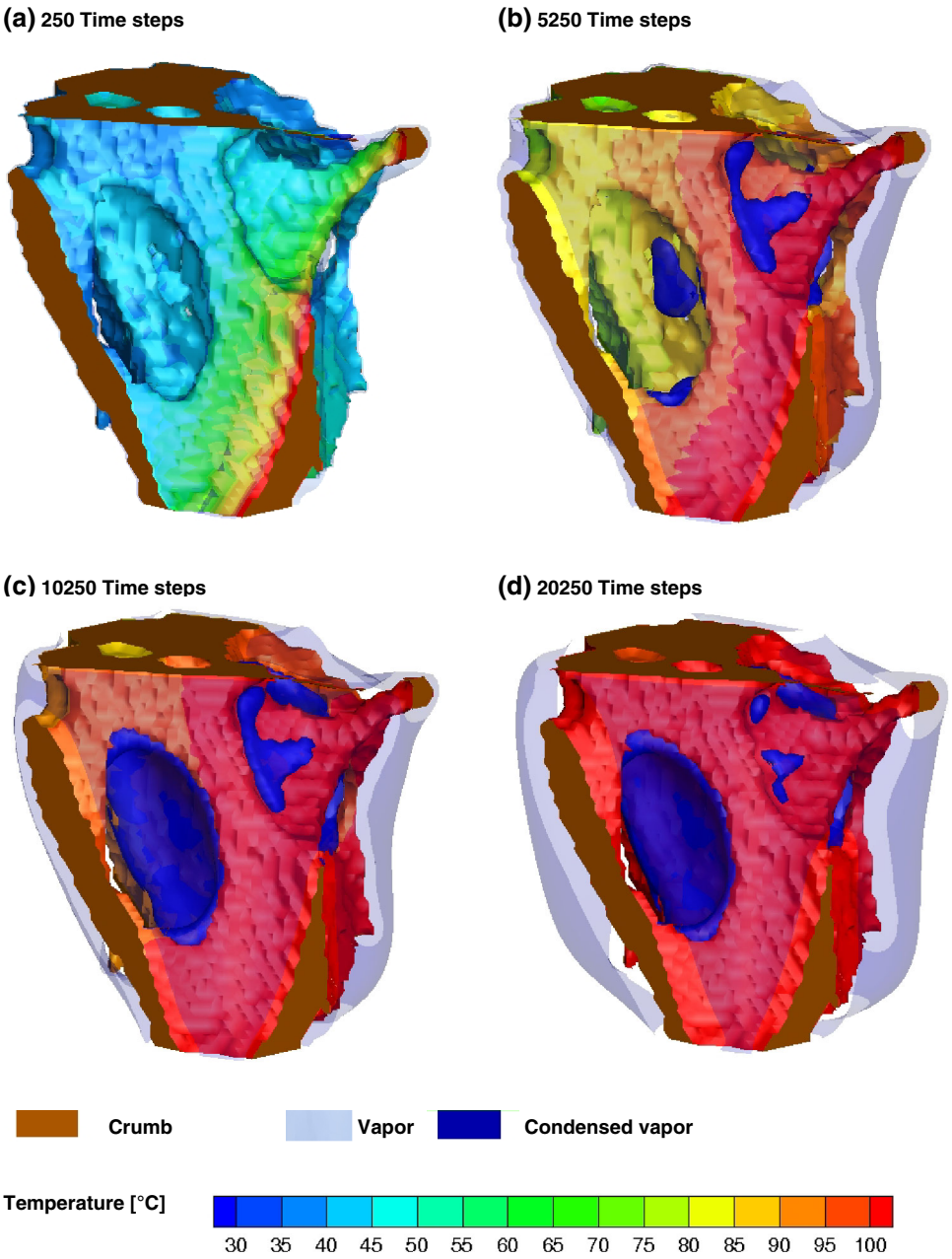

Fig. 5 Temperature distribution displayed at crumb surface in combination with the evaporation front in *gray-blue* and the development of condensed vapor shown in *dark blue* with proceeding time steps

evaporation–condensation heat transfer is dominant, then the amount of vapor and the possibility of its diffusion through the microstructure would influence the heat transfer. This is linked to the permeability of the foam lamella, the vapor diffusivity through the foam, and the free surface to bubble ratio leading to an increased evaporation rate. To estimate the ratio of thermal diffusion-driven heat transfer and combined evaporation–condensation heat transfer, the simulations are repeated under the same conditions but with neglecting the evaporation–condensation process. The results for both simulations, without evaporation–condensation and including evaporation–condensation, respectively, at a porosity of 72 % are plotted in Fig. 7.

The results show that indeed heat transfer proceeds quicker if evaporation–condensation is considered. Furthermore, the curve progression follows a steeper increase, meaning that for baking purposes, the conditions in the foam microstructure should be inside the range that evaporation–condensation takes place; thus, enough vaporizable water is present in the lamellas.

3.3 Parameter variation study

The next step covers the application of the proposed LB algorithm to determine the effect of microstructural variations on the heat transfer. The simulations are repeated for

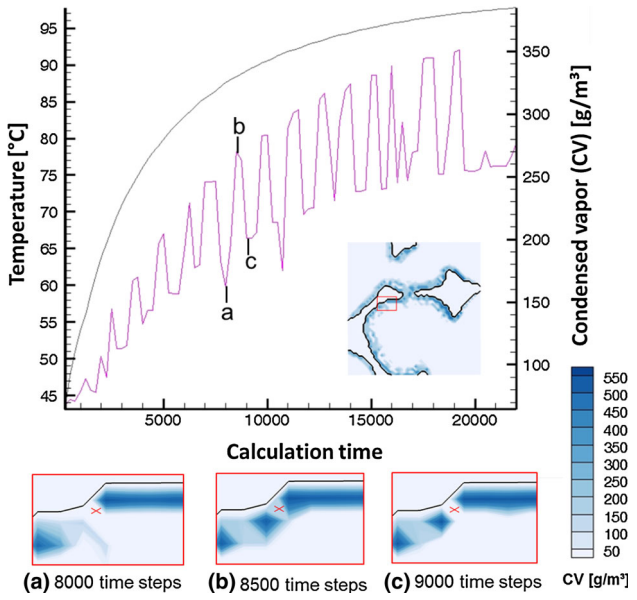

Fig. 6 Temperature and condensed vapor (CV) plotted versus calculation time. The *pink* curve shows the cyclic nature of the evaporation–condensation mechanism

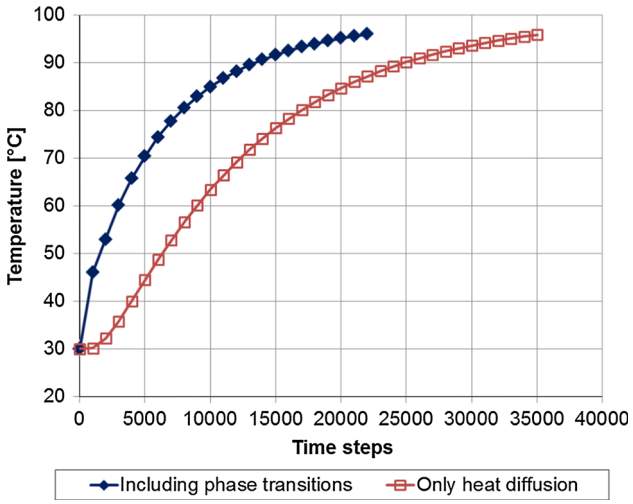

Fig. 7 Comparison of temperature progression dependent on solution time for simulations carried out including evaporation–condensation heat transfer and without considering such processes

different crumb microstructures, where the same µCT-images are uploaded in the Boltzmann code with increasing thresholds yielding in a different lamella to bubble ratio and therewith varied porosity (66.7–77.5 %). The simulation results are shown in Fig. 8, where the required time steps to reach a temperature of 98 °C, are plotted versus the crumb porosity.

The results show a linear decrease of required heating time with increasing porosity. Increasing porosity is linked to lamella thinning and increase of voids inside the lamellas. In conclusion, it can be suggested that such microstructural properties are responsible for the reduced heating time. Nonetheless, the applied edge detection algorithm used for the obstacle upload implies that these microstructural changes are related to a decrease in porosity and therewith a decrease of foam lamella mass in the computational domain. Thus, the heating time reduction may also be reasoned by this mass loss since the thermal diffusivity of the lamella is lower than through the bubble phase. To clarify the impact of the lamella configurations independent of lamella mass changes, artificial foam lamellas are generated having diverse amount of voids and increasing void size in combination with similar lamella mass in each variation case. Additionally, the thermal diffusivity of the foam lamella is varied to relate the possible heating time reduction of microstructural properties to

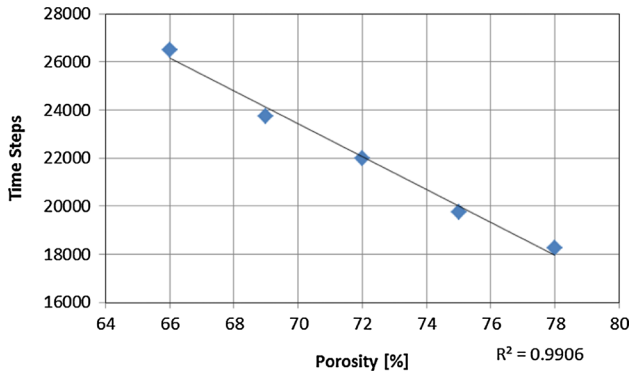

Fig. 8 Parameter variations of crumb porosity (thermal diffusivity remaining 0.157×10^{-6} m^2/s), showing that heating time increases with decreasing porosity

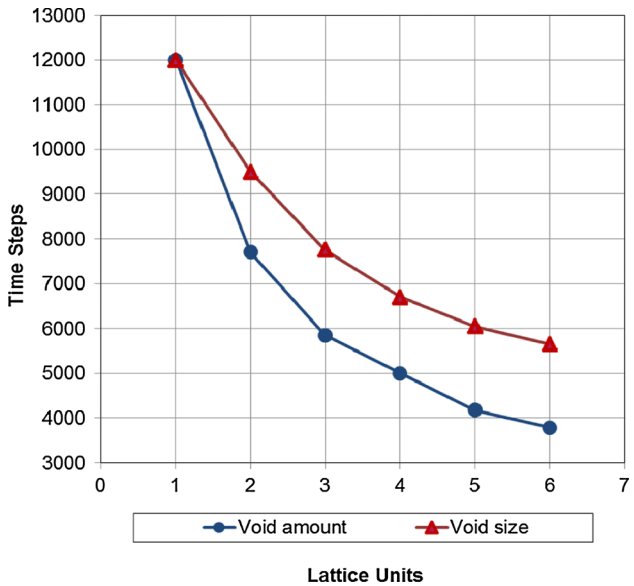

Fig. 9 Parameter variations of void amount and void size plotted in dependence of required time steps

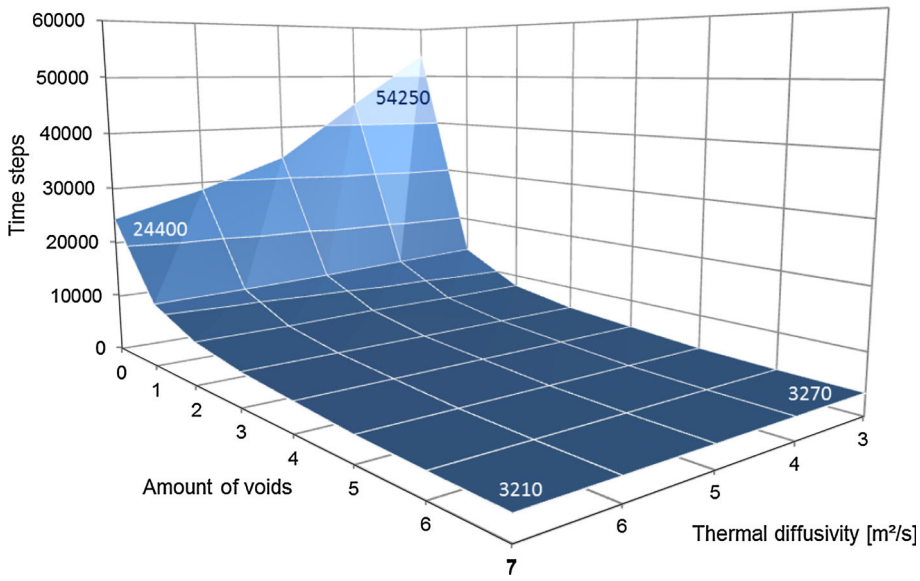

Fig. 10 Parameter variations of void number and thermal diffusivity of foam lamella in dependence of required heating time

material properties and to allow an estimation of the main influencing parameter. The simulation results for these individual foam lamellas are shown in Fig. 9.

The variations of amount and void size are carried out at a thermal diffusivity of the foam lamella of 0.157×10^{-6} m^2/s, the results show that with increasing void amount, and as well with increasing void size the required heating time decreases. This is reasoned by the increasing permeability of the foam lamella, allowing the vapor to diffuse with less resistance through the microstructure and thus yielding to a quicker heat spread. A further result of these variations is that the amount of voids has higher impact on the heat transfer then the size of a single void, where the amount of void space is kept similar in both cases. This effect is even rising with increasing void space. The reason for this progression may be the fact that increasing the amount of voids is linked to an increasing amount of free surface of the foam lamella thus enabling more vaporization from the lamella and therefore yielding to increased heat transfer by increased evaporation–condensation. The amount of free surface as well increases if the void size is increased but to a minor degree than in the case of increased amount of voids. The final part of the parameter variation study addresses the correlation of void number and thermal diffusivity of the foam lamella.

The results are shown in Fig. 10, where the amount of voids and the varied thermal diffusivity of each amount of voids are plotted versus the required time steps to finish the simulation. The results show that more time is required for a complete dense lamella and the lowest thermal diffusivity. Increasing the thermal diffusivity through such a dense lamella decreases the required heating time, but is still much higher than in the presence of voids. Generally speaking, increasing the amount of voids and increasing the thermal diffusivity yields to the quickest heat transfer. Worth to mention is that the impact of the thermal diffusivity of the lamella on the heating rate has a higher influence if fewer voids are present.

4 Conclusion

The LBM is used to enlighten the thermo-physical processes inside the microstructure of cereal foam. The results give insight into the coupled heat and mass diffusion as well as the linked phase transition processes of water inside the bubbles. It is shown that heat transfer in such microstructures is depending on evaporation–condensation heat transfer, besides thermal diffusion. In addition, the algorithm is used to deliver insight into the impact of microstructural properties on the heat transfer, and it could be shown that the main effect on heat transfer optimization is given by an increased amount of voids inside the foam lamellas. The presented results deliver the possibility how to optimize the heat transfer, but the conversion of these findings to an experimental continuation remains challenging. In this context, increasing the amount of free water in the dough seems to be straightforward from the simulation results but from a technological point of view simply increasing the amount of water would lead to production problems due to the specific water uptake of flours starch and thus different process conditions in worst case leading to a different final product. In conclusion, care has to be taken by the interpretation of the results by means of simply transferring the findings without considering the linked processes. But in spite of the challenge to convert the simulation results to a practical basis, the numerical investigations can be used to support the experimental heat

transfer optimizations in cereal foam showing the directions experimental research should focus on. Besides the conversion to an experimental basis, further work should be done to include the agglomeration of the condensed vapor phase to liquid water and the implementation of flow considerations of this liquid phase.

Acknowledgments This work was sponsored by the Deutsche Forschungsgemeinschaft DFG Grant Number: BE 2245/8-1. The authors thank Anja Dietrich, Fraunhofer Development Center X-ray Technology EZRT, Fraunhofer Institute for Integrated Circuits IIS, Fürth, Germany for the μCT-images.

References

De Vries U, Sluimer P, Bloksma AH (1989) A quantitative model for heat transport in dough and crumb during baking. In: Cereal Science and Technology in Sweden, Proceedings of an International Symposium. Sweden, Lund University, pp 174–188

Dietrich A, Nachtrab F, Salamon M, Khabta M, Uhlmann N, Hanke R (2012) Characterization of food foams using fast laboratory micro CT. In: Cellular materials—CELLMAT 2012, Dresden, Germany, 7–9 Nov 2012

Hussein MA, Becker T (2010) An innovative micro-modelling of simultaneous heat and moisture transfer during bread baking using the lattice Boltzmann method. Food Biophys 5(3):161–176

Mack S, Hussein MA, Becker T (2013a) Examination of thermophysical and material property interactions in cereal foams by means of Boltzmann modeling techniques. Microfluid Nanofluid 15:387–395

Mack S, Hussein MA, Becker T (2013b) Tracking the thermal induced vapor transport across foam microstructure by means of micro-sensing technology. J Food Eng 116(2):344–351

Perez Alvarado F, Hussein MA, Becker T (2011) Image processing in life science. In: Applications from cells to food. 10. Dresdner sensor-symposium, Dresden, Germany

Purlis E, Salvadori VO (2009) Bread baking as a moving boundary problem. Part 1: mathematical modelling. J Food Eng 91:428–433

Rask C (1989) Thermal properties of dough and bakery products: a review of published data. J Food Eng 9:167–193

Sablani SS, Marcotte M, Baik OD, Castaigne F (1998) Modeling of simultaneous heat and water transport in the baking process. Lebensm-Wiss u-Technol 31:201–209

Sluimer P, Krist-Spit CE (1987) Heat transport in dough during the baking of bread. In: Morton ID (ed) Cereals in a European context. Ellis Horwood, Chichester, UK, pp 355–363

Succi S (2001) The lattice Boltzmann equation for fluid dynamics and beyond. Oxford University Press, Oxford

Sukop MC, Thorne DT Jr (2007) Lattice Boltzmann modeling. An introduction for geoscientists and engineers. Springer, Berlin

Thorvaldsson K, Janestad H (1999) A model for simultaneous heat, water and vapour diffusion. J Food Eng 40:167–172

Thorvaldsson K, Skjöldebrand C (1998) Water diffusion in bread during baking. Lebensm-Wiss U-Technol 31:658–663

Wagner MJ, Lucas T, Le Ray D, Trystram G (2007) Water transport in bread during baking. J Food Eng 78:1167–1173

Wählby U, Skjöldebrand C (2001) NIR measurements of moisture changes in foods. J Food Eng 47:303–312

Wolf-Gladrow DA (2005) Lattice-gas cellular automata and lattice Boltzmann models—an introduction. Springer, Berlin

Zanoni B, Peri C (1993) A study of the bread-baking process. I: a phenomenological model. J Food Eng 19:389–398

Zhang J (2011) Lattice Boltzmann method for microfluidics: models and applications. Microfluid Nanofluid 10:1–28